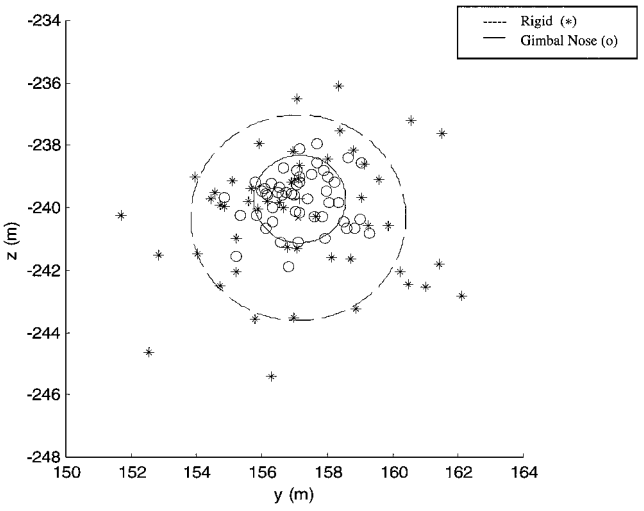

Fig. 3 Impact point dispersion at 3-km range.

variables with a mean of zero and standard deviation of 3 rad/s. A sample size of 50 simulations was used in computing impact point dispersion statistics. Figures 2 and 3 show the Monte Carlo simulation impact points for the baseline rigid and gimbal nose projectile configurations at a range of 1 and 3 km, respectively. In both charts, the circles correspond to a region such that 66% of the shot impacts fall within the circle. The large dashed circle corresponds to the rigid projectile whereas the small solid circle corresponds to the gimbal nose configuration. The dispersion circle radii for the rigid projectile at 1 and 3 km is 1.1 and 3.3 m whereas the dispersion circle radii for the gimbal nose projectile at 1 and 3 km is 0.5 and 1.4 m, respectively. Notice that the mean impact point of the two projectile configurations is different. The ratio of the dispersion circle radius for the gimbal nose to rigid projectile configuration is 0.43 and is independent of range. Thus, for the example penetrator projectile equipped with a gimbal nose, dispersion at any range can be reduced by a factor of 0.43.

Conclusions

A penetrator projectile equipped with a gimbal nose wind screen has the potential to reduce impact point dispersion drastically. By the mounting of the gimbal joint forward of the nose aerodynamic center, the nose tends to turn into the wind and reduces the sensitivity of the trajectory to launch disturbances. In the example case considered, impact point dispersion was reduced by more than 50%. The mean impact point of the rigid and gimbal nose projectile configurations are different, which will require fire control system logic to be modified depending on the particular projectile configuration being launched.

References

[1]Goddard, R. H., "Apparatus for Steering Aircraft," U.S. Patent 2594766, April 1952.

[2]Barrett, R., and Stutts, J., "Modeling, Design, and Testing of a Barrel-Launched Adaptive Munition," *Proceedings of the 4th Annual Society of Photo-Optical Engineers Symposium on Smart Structures*, Society of Photo-Optical Engineers, New York, 1997.

[3]Kranz, W., "High Velocity Aerodynamic Body Having Telescopic Nose Tip," U.S. Patent 4756492, July 1988.

[4]Schmidt, E., and Donovan, W., "Technique to Reduce Yaw and Jump of Fin-Stabilized Projectiles," *Journal of Spacecraft and Rockets*, Vol. 35, No. 1, 1998, pp. 110, 111.

[5]Murphy, C., "Free Flight Motion of Symmetric Missiles," U.S. Army Ballistic Research Lab., BRL Rept. 1216, Aberdeen Proving Ground, MD, July 1963.

[6]Angeles, J., *Fundamentals of Robotic Mechanical Systems*, Springer-Verlag, New York, 1997, pp. 28–30.

[7]Costello, M. F., and Anderson, D. P., "Effect of Internal Mass Unbalance on the Terminal Accuracy and Stability of a Field Artillery Projectile," *Proceedings of the 1996 AIAA Atmospheric Flight Mechanics Conference*, AIAA, Reston, VA, 1996.

Multi-Input, Multi-Output, Band-Limited Transducer Selection for Disturbance Rejection

Robert L. Clark*
Duke University, Durham, North Carolina 27708-0300
and
David E. Cox†
NASA Langley Research Center, Hampton, Virginia 23681-0001

Introduction

A BAND-LIMITED actuator/sensor selection methodology for disturbance rejection was previously developed.[1] Unlike prior methods, which emphasized disturbance rejection in selecting transducers that couple best to modes present in the performance path,[2–6] the methodology proposed by Clark and Cox[1] serves to further impose a penalty on the selection of transducer pairs that couple well to modes beyond the identified bandwidth of interest, creating a "natural" roll off in the frequency response from the selected spatial apertures of the transducers. In a more recent publication Smith and Clark[4] proposed a modification to the performance metric identified by Clark and Cox, providing a mechanism for selectively identifying modes to be controlled and modes to be ignored. Transducer pairs are chosen from a predetermined set based upon their selective coupling to identified modes for performance and lack of coupling to all other modes included in the model.

All of these design approaches are derived from the original work used in selecting actuator and sensor locations from a predetermined set of candidate locations based upon the Hankel singular values of the controllability and observability Gramians of flexible structures.[7,8] Within the original formulation, the actuator/sensor selection methodology was based entirely upon the Hankel singular values of the control path P_{yu} for some finite set of modes and some predetermined set of actuators and sensors.[7,8] Later revisions to this method have included a weighting of the Hankel singular values of the control path P_{yu} by that of the Hankel singular values of the performance path P_{zw} (Refs. 2 and 3). In the most recent extensions the actuator/sensor selection methodology based upon the disturbance rejection approach was modified with an additional metric aimed at robustness with respect to modes not targeted in the performance metric.[1,4]

A method of rank-ordering transducer pairs for control results from all of the design approaches is described.[1–8] Although the performance metrics allow the designer to select the best single-input, single-output (SISO) transducer pair from the predetermined target set, if more than one transducer pair is desired a multi-input, multi-output (MIMO) metric must be applied. The purpose of this Note is to introduce the MIMO design procedure and distinguish it from the SISO design approach. As will be demonstrated by example, one cannot simply select the rank-ordered SISO transducer pairs for the MIMO application when both in-bandwidth coupling and out-of-bandwidth roll off are part of the performance metric.

MIMO Band-Limited Placement Metric for Disturbance Rejection

For convenience the design problem can be cast in the standard two-port model as shown in Fig. 1. The upper transfer matrix $P_{zw}(s)$ represents the path from disturbances $w(s)$ to a measure of the system performance $z(s)$. This path is determined by the definition of

Received 27 December 1999; revision received 5 June 2000; accepted for publication 8 June 2000.

*Professor, Department of Mechanical Engineering and Materials Science, Box 90300. Member AIAA.

†Research Scientist.

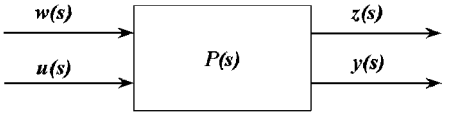

Fig. 1 Block diagram of the two-port design model.

the active control problem, with tradeoffs that reflect available resources (e.g., control energy) or robustness requirements. The lower transfer matrix $P_{yu}(s)$ represents the path from the control inputs $u(s)$ to the measured outputs $y(s)$ and is a function of the choice and placement of actuators and sensors respectively for the control system. Although usually taken as a given in control system design, often there is freedom determining sensor and actuator locations, yielding a design decision that impacts the resulting compensator design and closed-loop performance. Good placement for control design can be determined from the influence of transducers on the open-loop system's controllability and observability, measured in terms of the Hankel singular values.

Smith and Clark[4] introduced a performance metric used to determine the relative merit of the qth sensor and pth actuator:

$$J_{qp} = J^c_{qp} \Big/ J^{nc}_{qp} \tag{1}$$

where

$$J^c_{qp} = \sum_{i=1}^{n} \Xi_i \left(\frac{\gamma^4_{yqupi}}{\bar{\gamma}^4_{yui}} \right) \gamma^4_{zwi} \tag{2}$$

and

$$J^{nc}_{qp} = \sum_{i=1}^{n} \sim \Xi_i \left(\frac{\gamma^4_{yqupi}}{\bar{\gamma}^4_{yui}} \right) \gamma^4_{yqupi} \tag{3}$$

As detailed by Smith and Clark,[4] J^c_{qp} is the portion of the performance metric associated with the modes to be controlled, and J^{nc}_{qp} is the portion of the performance metric associated with the modes not to be controlled. γ^4_{yqupi} represents an estimate of the square of the Hankel singular value corresponding to the qth sensor, pth actuator, and ith mode, $\bar{\gamma}^4_{yui}$ represents an estimate of the square of the Hankel singular value over all possible sensors and actuators for the ith mode, and γ^4_{zwi} represents an estimate of the square of the Hankel singular value over all disturbance inputs and performance outputs for the ith mode. Details of the numerical estimation were provided by Lim and Gawronski,[7,8] and the estimation is restricted to systems with lightly damped modes. Ξ is a binary vector, and $\Xi_i = 1$ if the mode is targeted for control and 0 if not. Note that $\sim$ represents the binary not operator. As such, modes that were targeted for control in J^c_{qp} are now eliminated from the metric J^{nc}_{qp} used to impose roll off and minimize coupling to modes not required for performance. Dividing J^c_{qp} by J^{nc}_{qp} provides a relative measure of coupling to modes for performance against coupling to modes not desired in the control path. An ideal case would result in an actuator/sensor pair that coupled only to select modes. However, the typical result is a compromise.

A numerical value is computed for each actuator/sensor pair based upon the metric of Eq. (1), and the transducer pair with the highest metric is chosen for control system implementation. However, if more than one pair are required, one must either choose the two pairs with the higher values of the performance metric, a SISO design selection strategy, or develop a MIMO strategy. The problem with selecting the best SISO designs for MIMO application is that the cross terms in the system transfer matrix between control inputs and measured outputs for the MIMO system do not enter into the selection process. For example, if

$$P_{yu} = \begin{bmatrix} P_{yqup} & P_{yqus} \\ P_{yrup} & P_{yrus} \end{bmatrix}$$

the off-diagonal terms do not enter into the selection metric.

For a system with R candidate sensor locations and M candidate actuator locations, the optimal placement metric is

$$J^{\text{SISO}}_{\text{opt}} = \max_{q,\,p}(J_{qp})$$

$$q \in \{1, 2, \ldots, R\}, \quad p \in \{1, 2, \ldots, M\} \tag{4}$$

and the values of q and p at this maximum identify the corresponding optimal sensor and actuator locations. However, in the MIMO case it is not sufficient to iterate once over all sensors and actuator locations. The total number of unique choices that can define a single system with r sensors and m actuators is the product of the possible actuator combinations and sensor combinations and goes as

$$N_{\text{total}} = C_r \times C_m = \frac{R!}{r!(R-r)!} \times \frac{M!}{m!(M-m)!} \tag{5}$$

which reduces to a search space of $N_{\text{total}} = R \times M$ in the SISO case. The placement metric for the MIMO case must consider contributions for all paths within an actuator/sensor set,

$$J_n = \left(\sum_{i=1}^{m} \sum_{j=1}^{r} J_{q_j p_i} \right)$$

$$\bar{q} \in \left\{ \mathcal{S}_1, \mathcal{S}_2, \ldots, \mathcal{S}_{C_r} \right\}, \quad \bar{p} \in \left\{ \mathcal{A}_1, \mathcal{A}_2, \ldots, \mathcal{A}_{C_m} \right\} \tag{6}$$

where the elements $\mathcal{A}_{(\cdot)}$ and $\mathcal{S}_{(\cdot)}$ are themselves sets that contain unique collections of m actuators and r sensors, respectively. The MIMO optimum is simply

$$J^{\text{MIMO}}_{\text{opt}} = \max_{n}(J_n), \qquad n \in \{1, 2, \ldots, N_{\text{total}}\} \tag{7}$$

which also reduces to the SISO case. However, simply taking the top r sensor and m actuator locations from the SISO metric J_{qp} does not provide the same result, as it ignores cross terms from the double sum of Eq. (6).

N_{total} grows in a combinatorial fashion with the number of sensors and actuators. For more than a few transducers it becomes infeasible to find the maximum with a simple exhaustive search, and techniques for nonsmooth optimization[9] would be required to find an optimal, or near-optimal, choice. Here we focus on a small two-input two-output (TITO) problem and compare performance for the MIMO optimal transducer locations with the top two locations selected using the SISO metric.

Description of the Structural Model

In preparation for the design of an adaptive structure for control of turbulent boundary-layer noise, the actuator/sensor design methodology was applied to an approximate model of a system to determine the best target locations for the transducers. The test rig was constructed from aluminum and measured $0.508 \times 0.254 \times 0.0016$ m thick. The boundaries were constructed to approximate that of a plate with clamped boundaries, and piezoceramic transducers measuring $0.1524 \times 0.1016 \times 0.0002$ m thick were available for experimental implementation. In a previous study[9] transducers with large apertures were shown to provide desirable spatial wave-number filtering for control of low-frequency, long-wavelength, structural modes.

The model of the piezostructure was developed from an assumed modes approach as outlined by Clark et al.[10] The model included 60 states for the structural system, and there were 20 target locations for piezoceramic sensors (center points indicated by star symbols in Fig. 2) and 20 target locations for piezoceramic actuators (center points indicated by triangle symbols in Fig. 2). The schematic diagram of the plate and transducer center point locations is illustrated in nondimensional coordinates in Fig. 2. Based upon the target sensor and actuator locations, there are 400 unique SISO transducer pair options for design. In this example we choose to determine the best TITO array of transducers for control of the first, second, and third modes of the structure (i.e., $\Xi_{1,2,3} = 1$). A generalized disturbance capable of exciting all structural modes was created, and the performance was based upon the modal displacements associated with the first, second, and third structural modes.

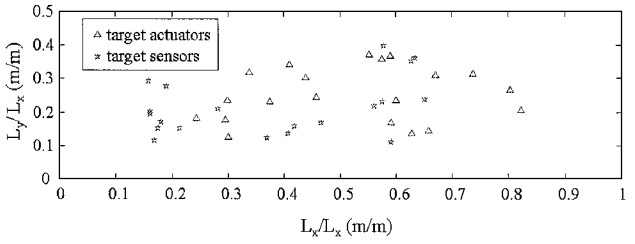

Fig. 2 Schematic diagram of plate with target actuator (triangles) and sensor (stars) center point locations.

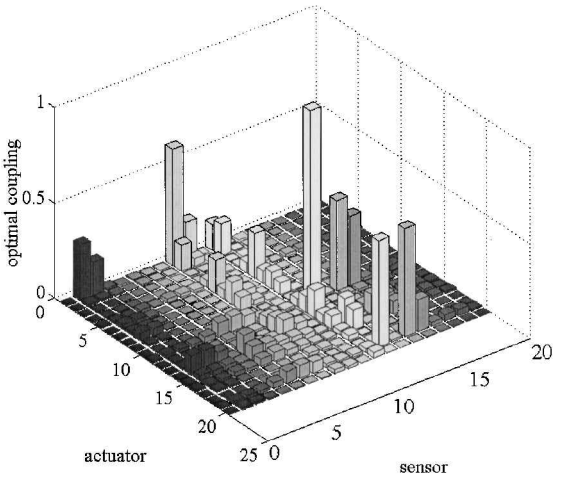

Fig. 3 Graphical presentation of performance metric evaluated for all target actuator/sensor locations.

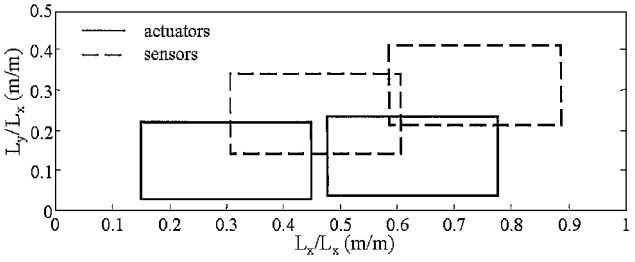

a) Best 2 SISO designs

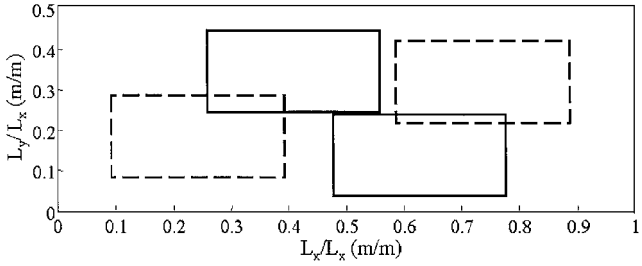

b) Best TITO design

Fig. 4 Schematic diagram of actuator and sensor locations based upon SISO and MIMO design metrics.

Results

The selection metric of Eq. (1) was used to rank order the SISO transducer options. The results are depicted graphically in Fig. 3. As illustrated, there are relatively few transducer pairs that satisfy both the level of coupling to the modes specified in the bandwidth as well as the desired level of decoupling or roll off imposed out of bandwidth. The top two SISO transducer pairs are illustrated in Fig. 4a. Implementing the MIMO design metric outlined in Eq. (7), the best TITO transducer pairs were chosen from all possible combinations of SISO pairs. As illustrated in Fig. 4b, the resulting design is different. Although the top SISO transducer pair was common to both designs, the secondary set of transducers was different.

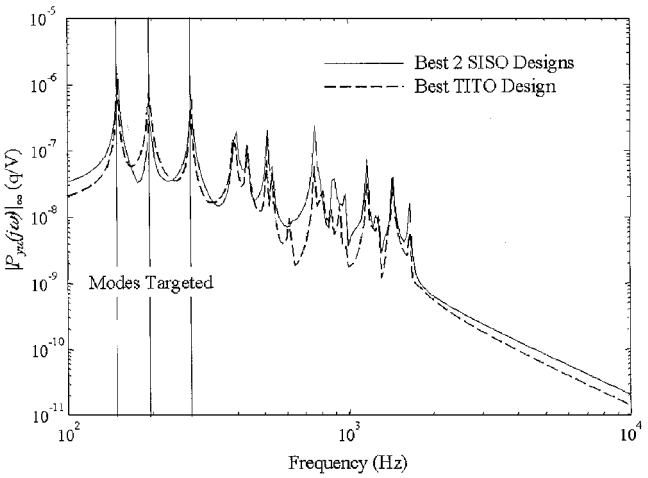

Fig. 5 Frequency response of MIMO systems resulting from the SISO design metric and the MIMO design metric.

The best way to compare the resulting designs is to quantify the maximum singular values of each design based upon the best two SISO designs illustrated in Fig. 4a and the best TITO design illustrated in Fig. 4b. The frequency response associated with the maximum singular values for each system (from control inputs to measured outputs P_{yu}) is presented in Fig. 5. The vertical lines are shown to indicate the modes targeted for control. In the bandwidth beyond these targeted modes, roll off or lack of coupling to higher order modes is desired. The solid line in Fig. 5 represents the frequency response associated with the system resulting from the best two SISO designs, and the dashed line represents the frequency response associated with the system resulting from the best TITO design. As illustrated, the best TITO design yields better coupling to the second structural mode (approximately 10 dB) and significantly less coupling to higher order modes than the system based upon the best two SISO designs. As a result, the MIMO design metric is obviously important if the objective is to maximize coupling to desired modes and minimize coupling to other modes in all transducer paths.

Conclusions

A MIMO band-limited actuator/sensor selection methodology for disturbance rejection was outlined. A structural design model was considered to compare the MIMO design strategy to a design strategy based upon selecting the best SISO transducer pairs. The results demonstrate that the performance metric is maximized for the MIMO system when all of the multivariable paths are considered in the design. As a result, the SISO transducer pairs having the highest performance metric will not necessarily correspond to the best MIMO transducer array. The design approach presented serves to extend the transducer selection methodology for crude multivariable loop shaping, enabling the structural engineer to better design a structure to be controlled.

References

[1]Clark, R. L., and Cox, D. E., "Band-Limited Actuator and Sensor Selection for Disturbance Rejection," *Journal of Guidance, Control, and Dynamics*, Vol. 22, No. 5, 1999, pp. 740–743.

[2]Lim, K. B., "Disturbance Rejection Approach to Actuator and Sensor Placement," *Journal of Guidance, Control, and Dynamics*, Vol. 20, No. 1, 1997, pp. 202–204.

[3]Lim, K. B., Lake, R. C., and Heeg, J., "Effective Selection of Piezoceramic Actuators for an Experimental Flexible Wing," *Journal of Guidance, Control, and Dynamics*, Vol. 21, No. 5, 1998, pp. 704–709.

[4]Smith, G. C., and Clark, R. L., "Adaptive Structure Design Through Optimum Spatial Compensation," *Proceedings of Active 99*, edited by Scott C. Douglas, Inst. of Noise Control Engineering, 1999, pp. 1013–1024.

[5]Gawronski, W., "Actuator and Sensor Placement for Structural Testing and Control," *Journal of Sound and Vibration*, Vol. 208, No. 1, 1997, pp. 101–109.

[6]Gawronski, W., *Dynamics and Control of Structures, A Modal Approach*, Springer-Verlag, New York, 1998, pp. 100–116.

[7]Gawronski, W., and Lim, K. B., "Balanced Actuator and Sensor Placement for Flexible Structures," *International Journal of Control*, Vol. 65,

No. 1, 1996, pp. 131–145.
[8]Lim, K. B., and Gawronski, W., "Hankel Singular Values of Flexible Structures in Discrete Time," *Journal of Guidance, Control, and Dynamics*, Vol. 19, No. 6, 1996, pp. 1370–1377.
[9]Ingber, A. L., "Adaptive Simulated Annealing (ASA): Lessons Learned," *Control and Cybernetics*, Vol. 25, No. 1, 1996, pp. 33–54.
[10]Clark, R. L., Saunders, W. R., and Gibbs, G. P., *Adaptive Structures: Dynamics and Control*, Wiley, New York, 1998, pp. 198–234.

Passive Nutation Control of Spinning Spacecraft Through the Use of Multiple Booms

F. O. Eke*
University of California, Davis, California 95616
A. Harvey†
Toyo Tanso USA, Inc., Troutdale, Oregon 97060
and
E. M. Eke‡
California State University, Sacramento, California 95819

Introduction

SEVERAL of the spacecraft in use today are spin-stabilized and are thus equipped with some form of nutation control system. Spacecraft nutation control devices can be active or passive. Passive nutation damping systems limit spacecraft nutation through onboard energy dissipation, and the design of such systems is based, for the most part, on well-established attitude stability criteria for spinning bodies.[1,2] When disturbed slightly from its position of stable spin, a spacecraft with internal energy dissipation will, in general, regain its original orientation faster than one without energy dissipation. This fact has led to the design of several passive devices that are triggered into dissipating energy onboard of a spacecraft anytime that the spacecraft attitude motion is disturbed. Such devices have included simple mass-spring-dashpot systems, damped physical pendulum, viscous fluid in ring-shaped tubes, etc.[3–5]

Spacecraft systems often include several rod-like appendages or booms attached to the main spacecraft bus, which serve various purposes during the vehicle's mission. In this study it is proposed to use two such booms on a given spacecraft for nutation control purposes. The idea is to replace the usual rigid attachment of such booms to the bus, with a one-degree-of-freedom hinge, together with a torsional spring and damper system. This effectively converts each boom into a pendulous damper for the spacecraft. Such arrangement differs markedly from the usual design of pendulous dampers in that the mass center of each boom would be outboard of the pivot point and the length would substantially exceed that of traditional pendulum dampers.

Motivation for this work comes from experience with the Galileo spacecraft,[6,7] where one such boom—its magnetometer boom—was used successfully as pendulous damper[8] to control spacecraft nutation. One area of concern for Galileo's single-boom damper design is stiction because of the small boom motions that are to be expected from such a damper design. Another is the possible deleterious effect of the dynamic imbalance that can result from the combination of spacecraft spin motions and boom deflection during thrusting, a phenomenon often referred to in the literature as wobble amplification.[9] In the case of Galileo, requirements on stiction were met without difficulty; however, wobble amplification was thought to pose enough danger to warrant the inclusion of a wobble control algorithm[7] in the attitude and articulation control subsystem.

The objective of this work is to explore the possibility of using more than one long pendulous boom as nutation damping device for spinning spacecraft. Specifically, we wish to study the effectiveness of using two identical pendulous booms arranged symmetrically with respect to the spacecraft's main bus as shown schematically in Fig. 1. There are two main potentially advantageous features of the proposed design. First, the symmetry of the arrangement eliminates, or at least drastically reduces, the imbalance or wobble amplification problem. The design also introduces some degree of redundancy in the nutation control system.

Equations of Attitude Motion

The physical system of interest is shown schematically in a general configuration in Fig. 1. A is the spacecraft's main bus, and B and C are booms that are connected to A through one-degree-of-freedom hinges. Stiffness and damping at the hinges are represented by the torsional spring and damper systems shown. Assuming that 1) A, B, and C are all rigid bodies; 2) A is uniform, homogeneous, and axisymmetric, with mass center at A^*; 3) B and C are identical, uniform, and homogeneous, with mass centers at B^* and C^*, respectively; the equations of attitude motion of the system are derived using the symbol manipulator software AUTOLEV.[10] The same software is also used to linearize these equations about the solution of pure spin, that is, a motion in which A spins about the zz' axis, and $\beta = \theta = 0$. The resulting equations are

$$\{I_A + 2I + 4m_A P^2 Z^2 + 2m[(L+Y)^2 + Z^2(2P-1)^2]\}\dot{u}_1 + [I + mL(L+Y)](\dot{u}_4 + \dot{u}_5) = \Omega\{I_A + 2J + 4m_A P^2 Z^2 - 2I - J_A - 2m[(L+Y)^2 - Z^2(2P-1)^2]\}u_2 + \Omega^2[J - I - mL(L+Y)](\beta + \theta) \tag{1}$$

$$\left[I_A + 2J + 4m_A P^2 Z^2 + 2mZ^2(2P-1)^2\right]\dot{u}_2 = -\Omega\left[I_A - J_A + 4m_A P^2 Z^2 + 2mZ^2(2P-1)^2\right]u_1 - J\Omega(u_4 + u_5) \tag{2}$$

$$[I + mL(L+Y)]\dot{u}_1 + \left[I - m_A L^2 P^2 + mL^2(1-2P^2)\right]\dot{u}_4 + mL^2 P\dot{u}_5 = \Omega[J - I - mL(L+Y)]u_2 - \sigma u_4 - \{K + \Omega^2[I - J + mL(L+Y)]\}\beta \tag{3}$$

$$[I + mL(L+Y)]\dot{u}_1 + mL^2 P\dot{u}_4 + \left[I - m_A L^2 P^2 + mL^2(1-2P^2)\right]\dot{u}_5 = \Omega[J - I - mL(L+Y)]u_2 - \sigma u_5 - \{K + \Omega^2[I - J - mL(L+Y)]\}\theta \tag{4}$$

and

$$\dot{u}_3 = 0 \qquad \text{or} \qquad u_3 = \Omega = \text{const} \tag{5}$$

where, in addition to the quantities shown in Fig. 1, I_A and J_A are, respectively, the transverse and spin central moments of inertia of A; I, and J are the corresponding inertia scalars for B or C; m_A is the mass of A; m is the mass of B or C; Ω is the constant spin rate of A under pure spin condition; and

$$P = m/(m_A + 2m) \tag{6}$$

Furthermore, the generalized speeds u_i $(i = 1, 2, 3)$ are the $\boldsymbol{a}_1, \boldsymbol{a}_2, \boldsymbol{a}_3$ scalar components of the inertial angular velocity of A, and u_4 and u_5 represent the respective angular speeds of B and C relative to the main body A. The preceding linearized dynamical equations can be supplemented with the kinematical differential equations

$$\dot{\beta} = u_4, \qquad \dot{\theta} = u_5 \tag{7}$$

The stability of the pure spin solution can be studied through eigenvalue analysis and leads straightforwardly to the determination of the time constant of the damper system.

Received 27 July 1999; revision received 13 March 2000; accepted for publication 1 June 2000.

*Associate Professor, Department of Mechanical and Aeronautical Engineering.
†Development Engineer, Engineering Department–Development Section, 2575 N.W. Graham Circle.
‡Professor, Department of Mechanical Engineering.